Redox-Dependent Structural Changes in the Superoxide Reductase from *Desulfoarculus baarsii* and *Treponema pallidum*: A FTIR Study†

Catherine Berthomieu,*,‡ François Dupeyrat,‡ Marc Fontecave,§ André Verméglio,‡ and Vincent Nivière§

CEA/Cadarache, DSV DEVM, Laboratoire de Bioénergétique Cellulaire, UMR 163 CNRS CEA, Univ-mediterranée CEA 1000, Bât. 156, F-13108 Saint-Paul-lez-Durance, Cedex, France, and Laboratoire de Chimie et Biochimie des Centres Redox Biologiques, DRDC-CEA/CNRS /Université J. Fourier, 17 avenue des Martyrs, F-38054 Grenoble, Cedex 9, France.

Received May 7, 2002; Revised Manuscript Received June 20, 2002

ABSTRACT: The redox-induced structural changes at the active site of the superoxide reductase (SOR) from *Desulfoarculus baarsii* and *Treponema pallidum* have been monitored by means of FTIR difference spectroscopy coupled to electrochemistry. With this technique, the structure and interactions formed by individual amino acids at a redox site can be detected. The infrared data on wild-type, Glu47Ala, and Lys48Ile mutants of the SOR from *D. baarsii* provide experimental support for the conclusion that the two different coordination motifs observed in the three-dimensional structure of the SOR from *Pyrococcus furiosus* [Yeh, A. P., Hu, Y., Jenney, F. E., Adams, M. W. W., and Rees, D. (2000) *Biochemistry 39,* 2499−2508] correspond to the two redox forms of the SOR iron center. We extend this result to the center II iron of SOR of the desulfoferrodoxin type. Similar structural changes are also observed upon iron oxidation in the SOR of *T. pallidum.* In *D. baarsii*, the IR modes of the Glu47 side chain support that it provides a monodentate ligand to the oxidized iron, while it does not interact with Fe^{2+}. Structural changes at the level of peptide bond(s) observed upon iron oxidation in wild-type are suppressed in the Glu47Ala mutant. We propose that the presence of the Glu side chain plays an important role for the structural reorganization accompanying iron oxidation. We identified the infrared modes of the Lys48 side chain and found that a change in its environment occurs upon iron oxidation. The lack of other structural changes upon the Lys48Ile mutation shows that the catalytic role of Lys, as evidenced by pulse radiolysis experiments [Lombard, M., Houée-Levin, C., Touati, D., Fontecave, M., and Nivière, V. (2001) *Biochemistry 40,* 5032−5040], is purely electrostatic, guiding superoxide toward the reduced iron.

Superoxide reductase (SOR)[1] is a recently discovered activity by which some anaerobic or microaerophilic organisms eliminate superoxide radicals, $O_2^{\bullet -}$ (*1*−*4*). SORs are non-heme iron proteins which catalyze the reduction of superoxide to hydrogen peroxide, by cellular reductases (*1*−*3, 5*):

$$SOR_{red} + O_2^{\bullet -} + 2H^+ \rightarrow H_2O_2 + SOR_{ox}$$

$$SOR_{ox} + 1e^- \text{ (cellular reductases)} \rightarrow SOR_{red}$$

In contrast to superoxide dismutase (SOD), which catalyzes the dismutation of superoxide into H_2O_2 and O_2, SOR activity does not result in O_2 production. SORs are involved in the resistance of the anaerobic bacteria to casual exposure to oxygen and allow them to settle in areas with very low oxygen concentration (*6*).

In most of these anaerobes, the hydrogen peroxide produced upon superoxide reduction can be converted to water via catalase (*7*) or specific enzymatic systems, e.g., NAD(P)H-dependent peroxidases, like peroxiredoxin (*8*), or rubrerythrin (*9, 10*). Although SOR is not naturally present in *Escherichia coli*, it was demonstrated that its expression in this bacterium could totally replace the SOD enzymes to overcome a superoxide stress (*3, 11, 12*). This strategy for eliminating superoxide without production of oxygen, using the reducing power of the cell, is an interesting alternative to prevent oxidative stress (*1, 2*). The simultaneous presence of both superoxide detoxification pathways, SOD and SOR, in some sulfate-reducing bacteria (*7, 13, 14*) suggests distinct roles for these enzymes and different regulatory systems. At the molecular level, one important issue concerns the mechanism by which the active site of SOR optimizes superoxide reduction and prevents or limits its oxidation, in contrast to SOD.

SORs can be divided into two major classes. The so-called homodimeric desulfoferrodoxin (Dfx) proteins are prototypes for the first class (*15, 16*). Dfx have been identified in *Desulfovibrio desulfuricans* (*15*), *Desulfovibrio vulgaris* (*16*),

† F.D. acknowledges a Ph.D. fellowship from the CEA and the PACA (Provence Alpes côte d'Azur) region. Part of this work was funded by the CEA: Program Toxicologie Nucléaire.

* Correspondence should be addressed to this author. Phone: 33 4 42 25 43 53, Fax: 33 4 42 25 47 01, E-mail: cberthomieu@cea.fr.

‡ CEA/Cadarache, DSV DEVM, Laboratoire de Bioénergétique Cellulaire.

§ DRDC-CEA/CNRS /Université J. Fourier.

[1] Abbreviations: SOR, superoxide reductase; SOD, superoxide dismutase; Nlr, neelaredoxin; Dfx, desulfoferrodoxin; (FT)IR, (Fourier transform) infrared; UV−Vis, UV−visible; XAS, X-ray absorption spectroscopy; EXAFS, extended X-ray absorption fine structure; PATS, pyridine-3-carboxaldehydethiosemicarbazone; dMPD, *N*,*N*-dimethyl-*p*-phenylenediamine; pBQ, 1,4-benzoquinone; TMPD, *N*,*N*,*N*′,*N*′-tetramethyl-*p*-phenylenediamine; DAD, 2,3,4,5-tetramethyl-*p*-phenylenediamine; PES, phenazine ethosulfate.

10.1021/bi020344x CCC: $22.00
Published on Web 07/19/2002

Scheme 1: Active Site of the SOR from *P. furiosus*, Determined from the Three-Dimensional Structure (*18*)[a]

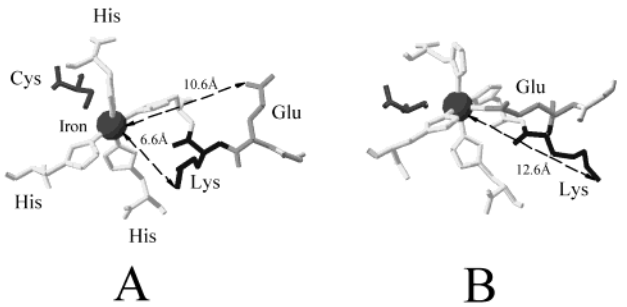

[a]Glu and Lys correspond to the Glu47 and Lys48 in the sequence of the SOR from *D. baarsii*.

and *Desulfoarculus baarsii* (*2*). In this class of SOR, the polypeptide chain consists of two domains, each containing a different mononuclear iron center (*17*). The C-terminal domain contains the active site with an Fe^{2+} center (center II) in an unusual [His_4 Cys_1] square pyramidal pentacoordination (*17*). Center II reacts with $O_2^{\bullet-}$ at a nearly diffusion-controlled rate, generating H_2O_2 and the oxidized form of the enzyme, with an Fe^{3+} center II (*2*). The N-terminal domain contains a desulforedoxin-like ferric center (center I), chelated by four cysteinyl sulfur ligands, with CysXXCysGly and CysCysGly iron binding motifs (*17*). As yet, the role of the iron center I in catalysis remains unclear (*2, 3*).

Homotetrameric neelaredoxin proteins (Nlr), such as that from *Pyrococcus furiosus* (*1, 18*), are prototypes for the second class. Each polypeptide contains only one non-heme iron center, structurally similar to the center II of Dfx. Nlr presents large sequence homologies with the C-terminal domain of Dfx but differs from it by the absence of a second domain binding the iron center I (*18*).

A third type of SOR, with high sequence homology to Dfx, but with only one iron center (center II), has been found in the spirochete *Treponema pallidum* (*3, 4*). The protein contains the second N-terminal domain but lacks three of the four cysteine residues involved in the chelation of the iron center I. This explains why this SOR might be classified as a Dfx rather than a Nlr (*3*).

Each class of SOR has been structurally characterized. However, there are still uncertainties as regards the iron coordination sphere in both oxidized and reduced forms. For the Nlr-type from *P. furiosus*, the crystallographic (*18*) and EXAFS (*19*) data suggest that in the reduced form, the ferrous center II is pentacoordinated, whereas in the oxidized form, the strictly conserved Glu14 provides an additional ligand to the ferric center (Scheme 1). This is a consequence of a local protein movement involving a small flexible loop including Glu14 and its neighbor Lys15 (*18*, Scheme 1). For the Dfx-type SOR from *D. desulfuricans*, the crystallographic characterization has been performed only on the oxidized form. At variance with *P. furiosus*, it does not reveal any electron density corresponding to a glutamate at the sixth coordination site (*17*). The nearest residues close to this vacant sixth coordination position are the strictly conserved Glu47 and Lys48, located at 7.5 and 10.5 Å, respectively (*17*) (this numbering is based on the SOR from *D. baarsii* and corresponds to Glu14 and Lys15 in *P. furiosus*).

Site-directed mutagenesis and pulse radiolysis studies on SORs have provided some insight into the enzyme mechanism. In particular, reaction intermediates following the reaction of $O_2^{\bullet-}$ with the active site have been detected in pulse radiolysis experiments (*20*−*23*) and were proposed to be iron peroxide species. That the SOR active site can indeed stabilize transiently such species was recently demonstrated by resonance Raman spectroscopy in the case of *D. baarsii* (*24*). Point mutations at the conserved Glu and Lys positions have been performed in SORs to analyze their respective role in superoxide reduction (*20*−*23*). In the SOR from *D. baarsii* (Dfx-type), the Lys48Ile mutation induces a 30-fold decrease of the rate of iron oxidation by superoxide (*21*). It has been proposed that Lys48 plays an important role for guiding $O_2^{\bullet-}$ to the sixth free coordination site of the ferrous center II (*21*). Accordingly, this mutation induces a decrease of the rescue property of the SOR gene when expressed in an *E. coli* strain deficient in SOD activity (*21*). On the other hand, mutations on the conserved Glu position have no or little effect on the rate of iron center oxidation by $O_2^{\bullet-}$, including the rate of formation of reaction intermediates detected in pulse radiolysis experiments (*20, 21, 23*). Nevertheless, resonance Raman studies on a Glu47Ala mutant of SOR from *D. baarsii* strongly suggest that this Glu residue is important for H_2O_2 release from the active site (*24*).

FTIR difference spectroscopy, combined with the electrochemical oxidation (reduction) of the iron center(s), can probe minute structural changes accompanying the change in redox state of the iron. The vibrations from individual amino acid side chains or peptide groups perturbed upon iron oxidation (reduction) can be identified (see *25*−*26* for reviews on the technique). The frequency and intensity of IR modes are sensitive to electrostatic and hydrogen bonding interactions of the vibrating group with its environment. Thus, information on the structure and interactions of individual amino acids at an active site, in particular the binding of carboxylates of Glu or Asp side chains with a metal, can be obtained (*27, 28*).

In this paper, we analyze by FTIR difference spectroscopy the redox-dependent structural changes at the iron centers of the SORs from *D. baarsii* and *T. pallidum*, taking advantage of the large difference in the midpoint potentials of center I and center II. In particular, we analyze the structural organization of Lys48 and Glu47 in reduced and oxidized center II of the SOR from *D. baarsii* and address the question of whether Glu47 is a ligand of the oxidized iron for this Dfx-type of SOR in solution.

MATERIALS AND METHODS

Recombinant SORs from *D. baarsii* wild-type, Glu47Ala, and Lys48Ile mutated forms were expressed in *E. coli* and purified as previously described (*21*). Purification of the recombinant SOR from *T. pallidum* was performed as described in (*3*). For FTIR spectroscopy, the proteins in 50 mM Tris-HCl buffer, pH 7.4, 100 mM KCl, and 20 mM $MgCl_2$ were concentrated to 1 mM using a Microcon 10 (Amicon).

Electrochemistry was performed in the thin-layer cell designed for FTIR spectroscopy (*29*), using a 4 μm thick gold mesh as a working electrode (Buckbee Mears, St. Paul,

MN). The electrode was coated with the modifier pyridine-3-carboxaldehyde thiosemicarbazone (PATS-3, purchased from Lancaster) by incubation for 5 min in a 5 mM solution of PATS-3 heated to 80−90 °C and subsequent washing thoroughly with 18 MΩ Millipore water. PATS-3 binds irreversibly to the gold surface through the sulfur atom and interacts with the proteins in solution through the pyridine and amine groups. The reference electrode consists of an Ag/AgCl/KCl (3 M) system (E_m = 208 mV/NHE). Thereafter, all the redox potentials are given versus NHE. A platinum counter-electrode at the periphery of the cell is used to compensate for the potential drop caused by the current. Electrochemistry was performed at 4 °C (6 °C in ^2H_2O) in the presence of the electrochemical mediators ferrocene (E_m = 422 mV), dMPD (E_m = 371 mV), pBQ (E_m = 280 mV), TMPD (E_m = 260 mV), DAD (E_m = 230 mV), PES (E_m = 55 mV), and duroquinone (DQ, E_m = 5mV), each at 40 μM final concentration. These mediators shuttle between the electrode surface and the redox centers of the protein, thus accelerating their electrochemical reduction (oxidation). The sample buffer and the mediators at this concentration did not contribute to the UV−visible or FTIR difference spectra (not shown). The potential was applied to the three-electrode system cell using an EG&G (model 362) potensiostat.

The redox titration of SOR centers I and II was performed by monitoring the potential-dependent UV−Vis absorption spectra, using the same electrochemical cell and conditions as for FTIR. The redox potential was changed by typical steps of 30 mV and absorption of the sample in the thin-layer cell recorded after equilibration, i.e., 6 min for center II and 10 min for the FeS_4 center I. The data were fitted with the Nernst equation using the Erytakus software Grafit. UV−Vis spectra were recorded with a Varian Cary 50 spectrophotometer.

FTIR spectra were recorded at 4 cm^{-1} resolution, with a Bruker 66 SX spectrometer equipped with a KBr beam splitter and nitrogen-cooled MCT-A detector. The absorption maximum of the sample was optimized at 0.85−0.9 au at 1645 cm^{-1}. Single-beam spectra recorded before and after a change of the redox potential were subtracted to calculate the redox-induced difference spectrum.

RESULTS

The electrochemical oxidation/reduction of iron centers I and II of the SOR from *D. baarsii* was performed, in both the UV−Vis and infrared domains, using the ≤10 μm path length electrochemical cell developed by D. Moss and W. Mäntele (*29*) for the study of proteins in aqueous media. The gold mesh electrode was coated with a surface modifier to avoid irreversible adsorption of the protein at the gold surface. Electrochemical mediators were added to the solution at concentrations below 1% of the protein concentration, to accelerate the electrochemical reaction.

In the experiment shown in Figure 1A, the SOR was totally oxidized when applying a potential of 600 mV, and the redox dependence of its absorption spectrum was studied in the +600 to −250 mV range (vs NHE). Both oxidized center I and center II exhibit absorption bands at 373 nm (*2*). The decrease of the absorption at 373 nm as a function of the redox potential can be fitted as the sum of two Nernst equations, with midpoint potential values of 432 and −7 mV

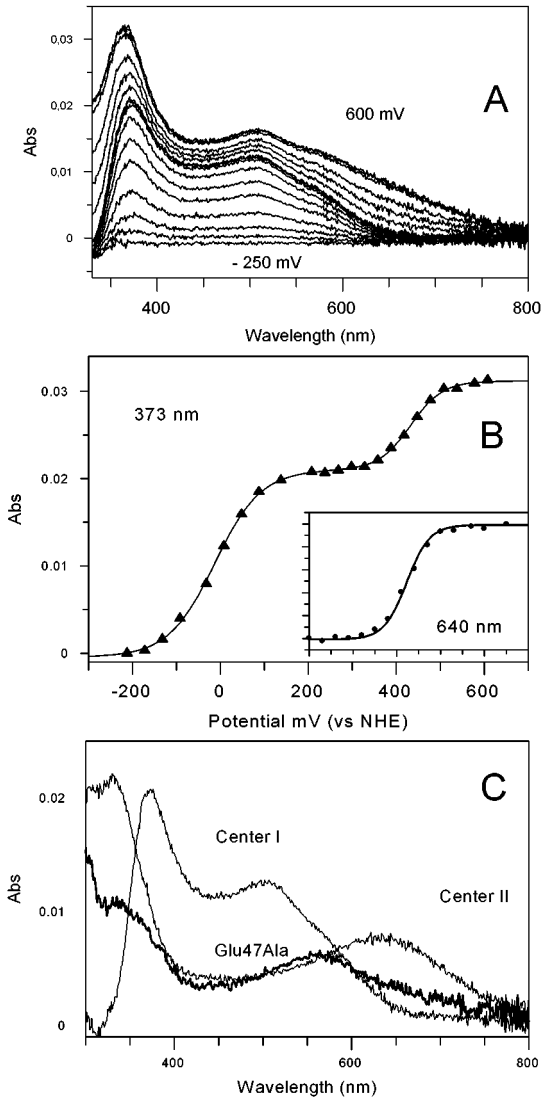

FIGURE 1: 1-A, absorption spectrum of the sample used for UV−Vis and FTIR spectroscopy at applied potentials varying from +600 mV (top) to −250 mV (bottom). 1-B, titration of the absorption at 373 nm (inset, at 640 nm) as a function of the applied potential. Line: curve-fit with a Nernst equation. 1-C, absorption spectrum of oxidized center I and center II in the SOR from *D. baarsii* WT and Glu37Ala mutant (boldface line)

(Figure 1-B). The decrease of the absorption at 640 nm, characteristic for the reduction of iron center II, can be fitted with a one-electron Nernst curve, with a midpoint potential of 430 ± 10 mV (Figure 1-B inset). This shows that the redox species with $E_m \approx -7$ mV corresponds exclusively to center I. The difference by more than 400 mV between the midpoint potentials of center I and center II allowed direct recording of the UV−Vis difference spectra corresponding solely to the oxidized centers I or II, as shown in Figure 1-C.

FTIR on Center I. In FTIR experiments, redox potential shifts between −200 and +200 mV and between + 300 and + 600 mV were applied to the SOR solution in order to study center I and center II independently. The FTIR difference spectra of the reduced minus oxidized form (boldface line) are shown in Figure 2-A and 2-B, for center I and center II of the SOR from *D. baarsii*, respectively. In these spectra, the signals correspond to changes in frequency and/or amplitude of IR modes of the groups affected by the

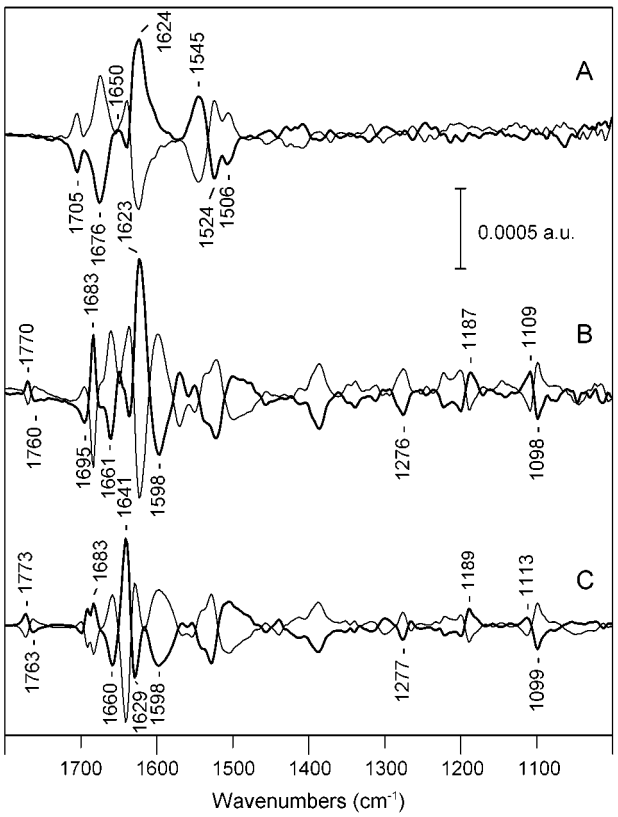

FIGURE 2: FTIR difference spectra corresponding to the reduced minus oxidized (boldface line) and oxidized minus reduced (thin line) FeS_4 center I (2-A) and SOR center II (2-B) of the Dfx from *D. baarsii*. Spectra in Figure 2-A have been obtained with oxidizing and reducing potentials of 200 and −200 mV, respectively, while spectra in Figure 2-B were obtained applying oxidizing and reducing potentials of 600 and 300 mV, respectively. Figure 2-C shows the reduced minus oxidized (boldface line) and oxidized minus reduced (thin line) FTIR difference spectra recorded with the SOR from *T pallidum*. For *T. pallidum*, oxidizing and reducing potentials of 400 and 0 mV have been applied. The spectra consist of an average of data recorded on 20−30 electrochemical cycles, 300 scans per cycle, 4 cm^{-1} resolution.

redox state of the active site iron. The negative bands (in the spectrum with boldface line) correspond to the oxidized state, and the positive bands correspond to the reduced state. The spectra for the oxidized minus reduced difference are also displayed in Figure 2 (thin line). The reversible symmetrical pattern indicates that all the bands correspond to structural reorganizations controlled by the redox state of the active site iron. Highly reproducible spectra are obtained.

The spectra of Figure 2-A and 2-B exhibit very different band patterns, which is consistent with the absence of contaminating contributions from one over the other center. In particular, in contrast to Figure 2-B, only very small potential-dependent IR bands are observed below 1500 cm^{-1} in Figure 2-A. Spectra from center I (Figure 2-A) show essentially contributions from peptide groups. The peptide ν(C═O) modes (amide I modes) are observed at 1676 cm^{-1} (for oxidized center I) and at 1650 and 1624 cm^{-1} (for reduced center I) while peptide ν(CN)+δ(NH) modes (amide II modes) contribute at 1545 cm^{-1} for reduced center I and at 1524 and 1506 cm^{-1} for oxidized center I. The dominant contribution of amide II modes in the latter region is supported by the almost complete disappearance of the signals upon $H_2O/^2H_2O$ exchange and the presence of signals at ≈100 cm^{-1} lower frequencies, corresponding to the amide II′ mode for the sample in ^2H_2O (not shown, *30*). The signal at 1705 cm^{-1} has a frequency compatible either with the IR mode of a peptide carbonyl or with the primary amide ν(C═O) mode of an asparagine side chain, possibly that of Asn15, located near the center I iron in the structure of SOR from *D. desulfuricans* (*17*).

The signals assigned to the peptide ν(C═O) IR modes in Figure 2-A result either from a decrease of the absorption amplitude or from a downshift by up to 50 cm^{-1} of the vibration frequencies (from 1676 cm^{-1} for oxidized center I to 1624 cm^{-1} for reduced center I) upon center I reduction. A frequency downshift of the ν(C═O) peptide mode corresponds to a decrease in the double bond character of the carbonyl group, i.e., to an increased electronegative character of the oxygen atom. The global frequency upshift observed for the amide II mode(s) from 1524 and 1506 cm^{-1} in the oxidized form, to 1545 cm^{-1} in the reduced form, are consistent with a shortening of the C−NH peptide bond concomitant with the increased electronegative character of the connected carbonyl oxygen. In center I, the iron is coordinated by the sulfur atoms of four cysteine side chains. Two ligands form hydrogen bonds with the NH groups of peptide bonds in a way similar to those existing in rubredoxin (*17*). The peptide IR modes observed in the spectra of Figure 2-A are assigned to the peptide groups, which are in NH···S hydrogen-bonding interaction with the iron−sulfur ligands (*17*). The frequency downshift of the ν(C═O) peptide modes observed upon iron reduction is interpreted as the result of the stabilization of the additional negative charge on the reduced iron by charge "delocalization" toward the carbonyl groups through the S···H bonds. This conclusion is drawn by analogy with a FTIR study performed on rubredoxin, for which a downshift by 30−40 cm^{-1} of ν(C═O) peptide modes (and concomitant upshift of amide II frequency) is the largest structural change observed upon iron reduction (B. Valentin, V. Bailleul, R. Kümmerle, J.-M. Moulis, and C. Berthomieu, in preparation). For the SOR from *D. baarsii*, increased electronegativity on the carbonyl oxygen could also occur for the peptide carbonyl of the two consecutive iron ligands Cys28 and Cys29 (*17*).

FTIR on Center II. In contrast to center I, spectra of center II (Figure 2-B) show signals in the whole spectral range, corresponding to peptide groups, which dominate in the 1700−1600 cm^{-1} region, and to amino acid side chains as well. In particular, bands at 1109/1098 cm^{-1} can be assigned to the ν(CN+CH) imidazole mode of histidine Nϵ ligands of the iron (*31*, *32*). Indeed, these signals, insensitive to $H_2O/^2H_2O$ exchange (Figure 3-A), have characteristic frequencies for side chain modes of histidine in interaction with a metal, as concluded from the analysis of protoporphyrin IX−imidazole model compounds and of ^{15}N-sensitive IR modes of histidine ligands of the non-heme iron of photosystem II (*31*, *32*). In both cases, the frequency and intensity of this histidine IR mode are sensitive to the oxidation state of the iron, being more intense with oxidized Fe^{3+} centers. ^{15}N-His labeling on FTIR difference spectra of the iron−plastoquinone electron acceptor complex of photosystem II provided evidence for other contributions from histidine ligands of Fe^{2+} at 1256 and 1179 cm^{-1} (*33*). These data suggest possible contribution of histidine side chain(s) in spectra of Figure 2-A at 1598 (Fe^{3+}), 1276 (Fe^{2+}), and 1187

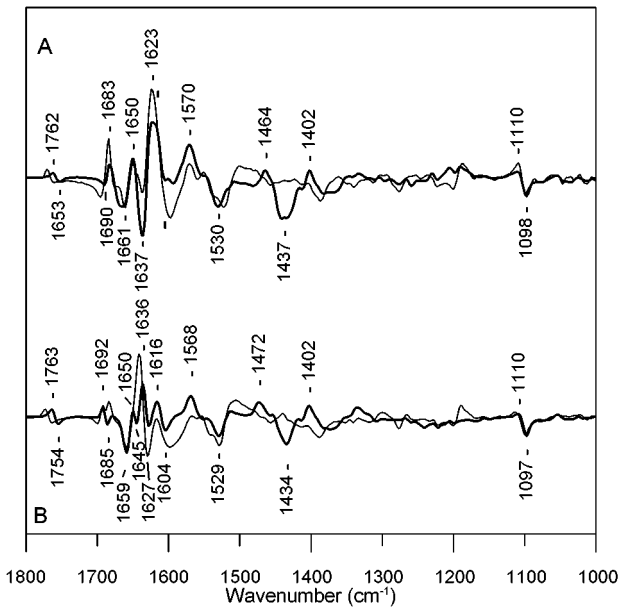

FIGURE 3: Comparison of reduced minus oxidized FTIR difference spectra for the SOR center II from *D. baarsii* (A) and the SOR from *T. pallidum* (B) in H_2O (thin line) and in ^2H_2O (boldface line). Peak frequencies are given for the spectra in ^2H_2O.

(Fe^{2+}) cm^{-1}. The differential signal observed at 1770/1760 cm^{-1} can be assigned without ambiguity to the protonated side chain of an Asp or a Glu residue (*34*, *35*). The frequency of this signal indicates that the carboxylic group is in a nonpolar environment. The 10 cm^{-1} downshift observed for this signal upon $H_2O/^2H_2O$ substitution (Figure 3-A) is also typical for a non-hydrogen-bonded carboxylic side chain (*36*).

SOR from T. pallidum. In this type of SOR, the iron center I is missing. The redox titration of the sample absorption at 660 nm can be fitted with a Nernst equation corresponding to a midpoint potential value of 290 ± 10 mV (not shown). Figure 2-C presents the FTIR difference spectra associated with the reduction (boldface line) or oxidation (thin line) of the iron center. These spectra present striking similarities with those of center II in the SOR from *D. baarsii*. These similarities are also evident for reduced minus oxidized spectra recorded in ^2H_2O (Figure 3, boldface line), in particular in the absorption region of carboxylate side chains (1530−1580 cm^{-1}). From this comparison, we can conclude that a similar electrostatic and structural reorganization occurs in the two proteins upon iron oxidation/reduction. This concerns the iron ligands with common signals assigned to histidine at 1113/1099 cm^{-1} and possibly at 1189 and 1277 cm^{-1}. It also concerns residues at greater distance from the iron, since the IR signal of a protonated Asp or Glu side chain, at 1773/1763 cm^{-1} in Figure 2-C, is observed for both SORs.

The largest differences between the FTIR difference spectra of Figure 3-A and 3-B are observed in the 1600−1700 cm^{-1} range, where peptide and amide ν(C═O) modes dominate the spectrum. Nevertheless, in this region, comparable signals are also observed at 1616, 1604, 1661(59), and 1650 cm^{-1}. Changes in hydrogen bonding strength formed by peptide carbonyls and slight differences at the level of the peptide backbone between the two SOR centers of *D. baarsii* and *T. pallidum* may account for the spectral differences at 1645(1637)/1636(1623) cm^{-1} and 1692+(1690−)/1685−(1683+) cm^{-1} in Figure 3-B(A).

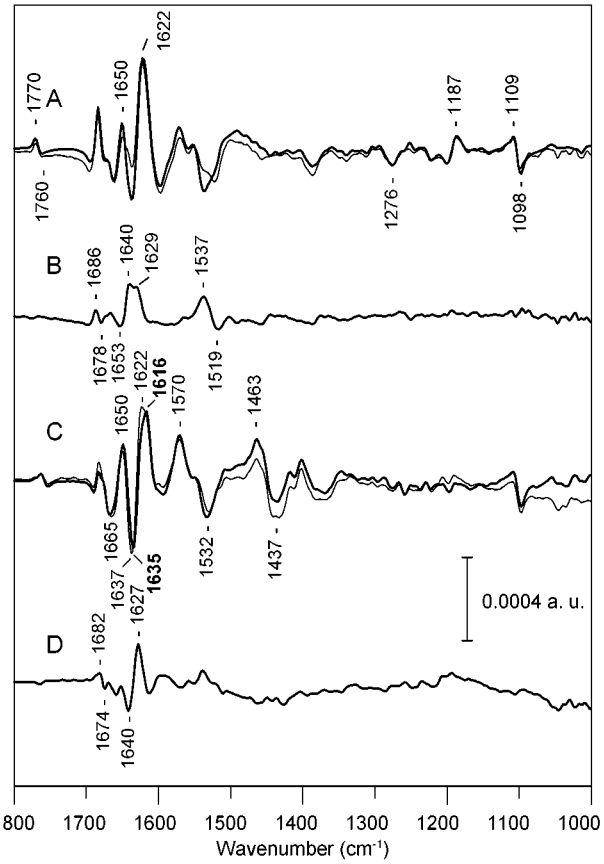

FIGURE 4: Effect of the Lys48Ile mutation on the FTIR difference spectra. Superimposition of the reduced minus oxidized FTIR difference spectra of the SOR center II from *D. baarsii* WT (thin line) or Lys48Ile mutant (boldface line) in H_2O (4-A) and in ^2H_2O (4-C). 4-C, difference spectrum WT minus Lys48Ile mutant in H_2O (calculated from spectra in 4-A). 4-D, difference spectrum WT minus Lys48Ile mutant in ^2H_2O (calculated from spectra in 4-C).

Lys48Ile Mutant. For the Lys48Ile mutant of the SOR from *D. baarsii*, the redox titration of the absorption spectrum in the UV−Vis domain locates the midpoint potentials of center I and center II at 448 ± 10 and ≈10 mV, respectively (data not shown). Figure 4 compares the reduced minus oxidized spectra obtained for center II with WT (thin line) and Lys48Ile mutant (boldface line) in H_2O (Figure 4-A) and in ^2H_2O (Figure 4-C). Most of the bands in the reduced minus oxidized FTIR spectrum are unchanged upon the Lys48Ile mutation. In particular, the signals at 1109/1098, 1187, and 1276 cm^{-1} are not affected. This is a strong indication that the coordination sphere of the iron, i.e., the charge distribution at the level of the iron ligands, is not significantly perturbed in this mutant. Also, the environment of the protonated Asp or Glu contributing at 1770/1760 cm^{-1} remains unaffected in the Lys48Ile mutant, showing that this residue is not in interaction with Lys48.

The bands altered in the reduced minus oxidized spectrum upon the Lys48Ile mutation can be visualized in the double difference spectrum (WT minus Lys48Ile) of Figure 4-B. They consist essentially of a differential band at 1653/1640 cm^{-1}, a positive signal at 1629 cm^{-1}, and a differential band at 1537/1519 cm^{-1}. Small changes also appear at 1686/1678 cm^{-1}. The side chain of isoleucine is not expected to contribute significantly to that spectrum (since aliphatic side chains have very small extinction coefficients), while the

lysine side chain and peptide group(s) may be observed. Discrimination between contributions from peptide amide I and amide II modes and from the ν_{as} and $\nu_s(NH_3+)$ modes of the Lys48 side chain in Figure 4-B can be achieved by comparison of spectra recorded in H_2O and in ^2H_2O, since the $^1H_2O/^2H_2O$ exchange is expected to affect differently the vibration frequency of these modes.[2]

The reduced minus oxidized FTIR difference spectra recorded in ^2H_2O for the WT and the Lys48Ile mutant are shown in Figure 4-C (thin and boldface lines, respectively), and the difference WT minus Lys48Ile mutant in ^2H_2O is displayed in Figure 4-D. Large signals in spectra of Figure 4-C at 1463/1437 cm^{-1} are due to amide II′ signals from ^2H-labeled peptide groups, which are almost identical for both WT and Lys48Ile mutant. In Figure 4-D, the bands at 1640/1627 cm^{-1} result from a slight downshift of amide I signals due to the Lys48Ile mutation with the negative band at 1637 cm^{-1} for the WT shifted to 1635 cm^{-1} for the Lys48Ile mutant and the positive band at 1622 cm^{-1} in the WT shifted to 1616 cm^{-1} in the Lys48Ile mutant (Figure 4-C). The effect at the level of a carbonyl ν(C═O) mode is expected for the spectra recorded in H_2O. Thus, the positive signal at 1629 cm^{-1} in Figure 4-B most probably corresponds to that at 1627 cm^{-1} in ^2H_2O.

The small differences at 1686/1678 cm^{-1} in H_2O (Figure 4-B), downshifted by 4 cm^{-1} to 1682/1674 cm^{-1} in ^2H_2O, are also assigned to a slight change at the level of the ν(C═O) mode of a peptide group, possibly that of the Lys or Ile. A downshift by less than 5 cm^{-1} upon $^1H/^2H$ exchange is consistent with the effect expected on peptide groups in hydrogen-bonding interaction.

The signals observed at 1653(−) and 1640(+) cm^{-1} in Figure 4-B (H_2O) are absent in the spectrum recorded in ^2H_2O. No signal can be assigned to the corresponding modes in ^2H_2O over the whole spectral range. A large frequency shift of these signals upon $^1H_2O/^2H_2O$ exchange is not consistent with the assignment to a peptide C═O group. In contrast, such a shift is expected for the $\nu_{as}(NH_3^+)$ mode of the lysine side chain, located at ≈1630 cm^{-1} in H_2O (*34*). Also, the changes observed at 1519 (−) and 1537 cm^{-1} (+) in Figure 4-B are absent in the difference spectrum recorded in ^2H_2O (Figure 4-D). We exclude a contribution from amide II bands at 1519/1537 cm^{-1} insofar as no corresponding signal is observed at 1460−1400 cm^{-1} for the expected corresponding amide II′ band in the difference spectrum of Figure 4-D. These signals can therefore be assigned with confidence to the $\nu_s(NH_3^+)$ mode of the lysine side chain, expected at ≈1526 cm^{-1} in H_2O (*34*). Thus, we propose that the ν_{as} and $\nu_s(NH_3^+)$ IR modes from the Lys48 side chain are responsible for the features at 1653 and 1519 cm^{-1} in the Fe^{3+} state and at 1640 and 1537 cm^{-1} in the Fe^{2+} state.

Glu47Ala Mutant. For the Glu47Ala mutant, the redox titration of the absorption spectrum locates the midpoint potential of center II at 488 ± 10 mV (not shown). The midpoint potential for center I is not affected by the mutation. The spectrum of the oxidized center II is largely different from that of WT (Figure 1-C), with the maxima at 640 and 370 nm blue-shifted to 560 and 340 nm in the Glu47Ala mutant. The extinction coefficients of the two bands are smaller, in particular for the band at ≈340 nm, which is at least 2 times smaller than in the WT. The spectrum we obtained was very similar to that observed when the mutant was oxidized with superoxide (maximum at 580 nm, *21*) and identical to that obtained when the mutant was oxidized with iridium(IV) hexachloride (*24*).

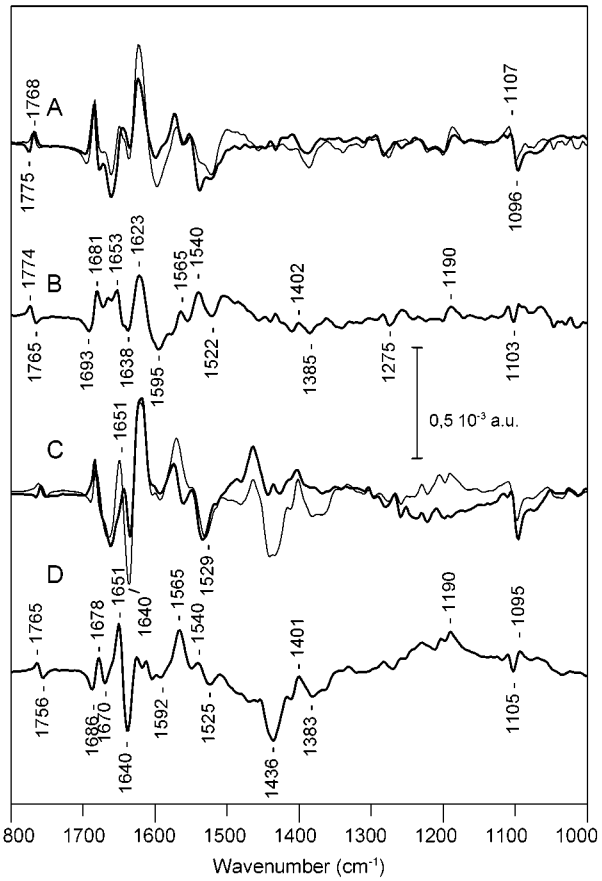

FIGURE 5: Effect of the Glu47Ala mutation on the FTIR difference spectra. Reduced minus oxidized FTIR difference spectra of the SOR center II from *D. baarsii* recorded with WT (thin line) and the Glu47Ala mutant (boldface line) in H_2O (5-A) and ^2H_2O (5-C). Difference spectrum WT minus Glu47Ala mutant in H_2O (5-B) and ^2H_2O (5-D).

Several significant changes are observed in the infrared region for center II upon Glu47Ala mutation (Figure 5-A in H_2O and 5-C in ^2H_2O). The differences are shown in the WT minus Glu47Ala difference spectrum of Figure 5-B. In contrast to that observed with the Lys48Ile mutant, the IR mode at 1107/1096 cm^{-1} assigned to histidine ligand(s) is slightly downshifted in the Fe^{3+} state and has a larger intensity as compared to the WT (1109/1098 cm^{-1}). Changes in signal intensity and frequency are also observed at 1595, 1275, and 1190 cm^{-1} in Figure 5-B, that may also be assigned to perturbation of side chain modes of the histidine ligands. The IR signal assigned to a protonated Asp or Glu at 1770(+)/1660(−) cm^{-1} is displaced to 1768(+)/1775(−) cm^{-1} in the spectrum recorded with the Glu47Ala mutant (Figure 5-A). This change corresponds to a significant upshift upon Glu47Ala mutation of the negative signal, due to the carboxylic group in the Fe^{3+} state, while the frequency is almost unchanged in the Fe^{2+} state.

Two characteristic IR modes are expected for the carboxylate side chain of glutamate, the $\nu_{as}(COO^-)$ mode at

[2] Band shifts of several hundreds of cm^{-1} are expected for the lysine side chain modes (*35*), while amide I modes are downshifted by up to 15 cm^{-1} and amide II modes are downshifted by ≈100 cm^{-1} (*30*).

≈1560 cm^{-1} (1566−1570 cm^{-1} in ^2H_2O) and the $\nu_s(COO^-)$ mode at ≈1400 cm^{-1} (*34, 37*). For a glutamate forming a monodentate metal ligand, the frequency of the $\nu_{as}(COO^-)$ is upshifted, by comparison with (free) anion in solution, while the $\nu_s(COO^-)$ mode may be downshifted, although this mode is usually less affected upon binding (*27, 28*). The resulting frequency difference $\nu_{as} - \nu_s$ (COO^-) larger than for ionic carboxylate is typical for monodentate binding (*27*).

In the difference spectrum WT minus Glu47Ala mutant, obtained in H_2O (Figure 5-B), a small positive band appears at 1565 cm^{-1} together with a differential signal at 1540/1522 cm^{-1} in the absorption region for $\nu_{as}(COO^-)$ groups. No clear negative signal in this range can be assigned to the $\nu_{as}(COO^-)$ mode of Glu47 in the oxidized Fe^{3+} state. This region is complicated in H_2O, due to possible contributions from amine or amide II modes. Therefore, the spectra were recorded in ^2H_2O (Figure 5-C), and the difference spectrum WT minus Glu47Ala is shown in Figure 5-D. No or small upshifts by a few wavenumbers are expected on the frequency of carboxylate $\nu_{as}(COO^-)$ upon $^1H_2O/^2H_2O$ exchange, while the frequency from amide II or R−NH_x groups is downshifted by at least 100 cm^{-1}. Also, the intensity of the $\nu_{as}(COO^-)$ mode is almost twice larger in ^2H_2O than in H_2O (*34, 35, 37*). In Figure 5-D, a positive signal emerges at 1565 cm^{-1}, which is the only possible candidate for the Glu47 $\nu_{as}(COO^-)$ side chain mode in the Fe^{2+} state. The small difference band at 1540/1525 cm^{-1} results from the 5 cm^{-1} upshift of the negative band at 1529 cm^{-1} in ^2H_2O in WT upon mutation (Figure 5-C). This difference signal at 1540/1525 cm^{-1} is most probably equivalent to that at 1540/1522 cm^{-1} in H_2O (Figure 5-B). In Figure 5-D, the negative signals that could be assigned to the Glu47 side chain in the Fe^{3+} state are above the region for ionic carboxylate IR modes, with possible contributions at 1592−1606, 1640, 1670, or 1686 cm^{-1}. All these frequencies would correspond to a carboxylate engaged in monodentate metal coordination. The difference spectrum obtained in ^2H_2O also shows possible candidates for the $\nu_s(COO^-)$ mode of Glu47 side chain at 1401 and 1383 cm^{-1} for the Fe^{2+} and Fe^{3+} states, respectively (Figure 5-D). In H_2O, these modes may contribute at 1402 and 1385 cm^{-1}, respectively, in the Fe^{2+} and Fe^{3+} states.

The positive band at 1565 cm^{-1} is probably partly masked in the spectrum recorded in H_2O by a large negative signal at 1570−1550 cm^{-1} from an amide II band, which is displaced and yields the large negative band at 1436 cm^{-1} in ^2H_2O (Figure 5-D). This band refers to a change in peptide conformation upon iron oxidation in the WT which does not exist in the Glu47Ala mutant, either at the Glu47 peptide group or at amino acid(s) in its vicinity. Accordingly, a difference band at 1651(+)/1640(−) cm^{-1} in the spectrum in ^2H_2O for the WT (Figure 5-C thin line), which can be assigned to the ν(C═O) mode of a peptide group, is absent in the spectrum recorded with the mutant (Figure 5-C boldface line). This signal corresponds to a structural change upon iron oxidation in the WT, possibly involving more than one peptide group and influenced by Glu47. The data in Figure 5-D show that the presence of the Glu47 side chain is required to induce this structural reorganization upon iron oxidation.

DISCUSSION

In this work, we have investigated the redox-induced structural changes of the active site of the SOR from *D. baarsii* and *T. pallidum* by means of electrochemically induced FTIR difference spectroscopy. With this technique, very small structural perturbations or changes in charge repartition at the metal centers as well as long-range repercussions in the protein are detected. The difference, in our experimental conditions, of more than 400 mV between the midpoint potential of iron centers I and II, of the SOR from *D. baarsii*, has allowed us to study center I and center II independently during oxido-reduction processes. In addition, studies on the two SOR mutants, Lys48Ile and Glu47Ala, have permitted us to unambiguously assign various bands observed in the wild-type SOR.

Comparison of FTIR Difference Spectra Obtained with WT and Glu47Ala Mutant. The Glu47Ala mutation induces a large number of spectral changes in the infrared. The $\nu_{as}(COO^-)$ mode of Glu47 is assigned at 1565 cm^{-1} in the Fe^{2+} state, which corresponds to a noncoordinated ionic glutamate (*34*). In the Fe^{3+} state, although the frequency of the $\nu_{as}(COO^-)$ mode cannot be identified with confidence, the data allow us to rule out any contribution in the spectral range where ionic carboxylates, unbound to metal, are expected to absorb. The frequencies, at 1693 (1686 in ^2H_2O), 1638−1640, or 1592−1606 cm^{-1}, all correspond to carboxylate as a monodentate ligand of Fe^{3+}. Thus, the IR data support the view that Glu47 is a monodentate ligand of the oxidized center II iron, while it does not interact with the reduced metal.

In the case of the SOR from *P. furiosus*, the presence of a monodentate Glu14 occupying the sixth coordination position of the oxidized center, whereas it is not a ligand in the reduced form, has been suggested by the three-dimensional structure and by recent EXAFS studies (*18*, *19*). Our FTIR results clearly demonstrate that such a coordination change also occurs in the Dfx-type of SOR, with the Glu47 being a ligand in the oxidized ferric form on the iron center II, but not in the reduced form. This seems at first sight in contradiction with the crystal structure of the oxidized Dfx from *D. desulfuricans*, which revealed no density at the sixth coordination position (*17*). Recently, XAS experiments on the SOR from *P. furiosus* showed that iron reduction occurs rapidly under the X-ray beam (*19*). As suggested by the authors, this might have happened also during the exposure of the crystal of the Dfx from *D. desulfuricans* to the X-rays. Our present data also strongly suggest that the crystal structure of the Dfx from *D. desulfuricans* corresponds to the reduced form (*17*).

In addition, our data show that a conformational change detected at the level of at least one peptide group for the wild-type SOR upon reduction/oxidation is canceled by the Glu47Ala mutation. We attribute this signal to a structural reorganization at the level of the Glu47 peptide bond or that of a neighboring residue in the flexible loop described by the X-ray crystallography (*17*). The FTIR data show that the Glu side chain is necessary to initiate this structural reorganization between reduced and oxidized iron.

The mutation at Glu47 induces other perturbations of the FTIR difference spectrum associated with the iron oxidation (reduction). In particular, the differential signal assigned to

the histidine Nϵ ligands of the iron is downshifted to 1107/1096 cm^{-1}, indicating an increase of the electronic charge on the histidine ligand(s), when compared to the WT protein. This might be in line with the increase of the iron midpoint potential by more than 60 mV in the Glu47Ala mutant.

Comparison of Spectra Obtained with WT and Lys48Ile Mutant. In contrast, only very limited structural changes are observed upon Lys48Ile mutation in the FTIR difference spectra corresponding to SOR center II oxidation. The IR changes concern mainly the Lys side chain modes: the ν_{as} and $\nu_s(NH_3^+)$ IR modes identified at 1653 and 1519 cm^{-1} in the Fe^{3+} state and at 1640 and 1537 cm^{-1} in the Fe^{2+} state. The extinction coefficients of the IR modes of lysine in the Fe^{2+} state are at least twice larger than the corresponding modes identified in the Fe^{3+} state, and larger than the typical extinction coefficients of these modes reported at 130 and 100 $\pm$ 10 $L \cdot mol^{-1} \cdot cm^{-1}$, respectively, as compared to the intensity of the Glu47 $\nu_{as}(COO^-)$ mode in ^2H_2O (*34*, *38*). The large intensity of the Lys side chain mode observed in the Fe^{2+} state can be due to a strong electrostatic interaction, between the lysine side chain and the coordination sphere of the iron. Thus, the IR data support the presence of an interaction between the Lys side chain and the center II iron in reduced SOR, while this interaction is decreased in the Fe^{3+} state. A change in the environment of the Lys side chain upon iron oxidation is also apparent from the larger frequency difference detected between the ν_{as} and $\nu_s(NH_3^+)$ Lys modes (+31 cm^{-1}) in the Fe^{3+} state than in reduced SOR. The IR data are thus in agreement with the reorientation of the Lys side chain at an increased distance from the iron upon Fe oxidation, as shown in the crystal structure of the SOR from *P. furiosus* (Scheme 1, *18*).

The lack of large differences in the amide I and amide II regions between the FTIR difference spectra recorded with WT and the Lys48Ile mutant shows that the structural changes that accompany the iron oxidation in WT are conserved in the mutant. As viewed by FTIR, the Lys48 side chain is not at the origin of these structural rearrangements. Thus, the critical role of Lys48 in $O_2^{\bullet -}$ guiding to the reduced iron, evidenced by pulse radiolysis experiments (*21*), is a pure electrostatic role due to the charge of its side chain.

Comparison of the SORs from D. baarsii and T. pallidum. Large similarity is observed between the redox-induced structural changes in center II of the SOR from *D. baarsii* and the active center of the SOR from *T. pallidum*. The IR modes of the histidine iron ligands appear at only slightly different frequencies. In particular, the high similarity in the absorption region for carboxylate groups in ^2H_2O (Figure 3) suggests that the conversion from ionic to monodentate of the Glu ligand also occurs upon iron oxidation in the SOR from *T. pallidum*.

For both *T. pallidum* and *D. baarsii* SOR centers, a difference signal at 1770/1760 cm^{-1} is assigned to a conformational change at the level of a protonated Asp or Glu side chain upon iron oxidation. The high vibration frequency of this carboxylic group and the frequency downshift observed upon $H_2O/^2H_2O$ exchange indicate that this group is not hydrogen-bonded. Also, for ν(C=O) frequencies above 1740 cm^{-1}, an inverse correlation between the ν(C=O) frequency and the dielectric constant, ϵ, of the medium has been reported (*39*). The observed frequency corresponds to a dielectric constant below or equal to 2, i.e., corresponding to neighboring aliphatic side chains. In the structure of the SOR from *D. desulfuricans*, among the Asp and Glu side chains, only that of Glu113 is buried in the protein (*17*). This glutamic residue sits below the active site center II iron, at $\approx$7 Å from the iron in a hydrophobic environment. This residue is conserved in the SOR from *D. baarsii* (*2*) and in that of *T. pallidum* (*3*). Therefore, we assign the difference band at 1770/1760 cm^{-1} (1773/1763 cm^{-1} for *T. pallidum*) to the protonated side chain of this Glu113.

The Glu47Ala mutation perturbs the IR difference signal assigned to Glu113. The largest effect is the upshift of the IR mode in the oxidized SOR center. These FTIR data show that the absence of the sixth Glu ligand on the oxidized iron modifies the dielectric constant in the environment of the Glu113. With respect to Glu47, Glu113 is located at the opposite site from the plane formed by the iron and histidine ligands. This long-range electrostatic effect between Glu47 and Glu113 underlines a property of the iron site that may be relevant to the protein function. Moreover, it should be noted that Glu113 is not conserved in the sequence of SORs of the Nlr-type, whereas it is present in most of the Dfx-type from eubacteria (*3*). We intend to design site-directed mutants at this position to evaluate the influence of this group in the SOR reactivity.

The midpoint potential of the SOR from *D. baarsii*, at 430 mV, is higher by about 140 mV than that of *T. pallidum* determined at 290 mV by spectro-electrochemistry. Differences in the redox-induced structural changes observed by FTIR between the two SOR centers cannot be assigned to a specific amino acid side chain. These differences essentially concern the peptide backbone. The difference in midpoint potential may also be due to slight differences in iron−cysteine interactions. Indeed, the IR frequencies of Cys, expected below 1000 cm^{-1}, could not be identified in the present study. A detailed study of the influence of Cys in the properties of the SOR center will be undertaken in WT and site-directed mutants, using an infrared cell adapted for the low-frequency region.

ACKNOWLEDGMENT

A. Boussac, Rainer Hienerwadel, and Jérome Lavergne are gratefully acknowledged for discussions and reading of the manuscript.

REFERENCES

1. Jenney, F. E. Jr., Verhagen, M. F. J. M., Cui, X., and Adams, M. W. W. (1999) *Science 286*, 306−309.
2. Lombard, M., Fontecave, M., Touati, D., and Nivière, V. (2000) *J. Biol. Chem. 275*, 115−121.
3. Lombard, M., Touati, D., Fontecave, M., and Nivière, V. (2000) *J. Biol. Chem. 275*, 27021−27026.
4. Jovanovic, T., Ascenso, C., Hazlett, K. R. O., Sikkink, R., Krebs, C., Litwiller, R., Benson, L. M., Moura, I., Moura, J. J. G., Radolf, J. D., Huynh, B. H., Naylor, S., and Rusnak, F. (2000) *J. Biol. Chem. 275*, 28439−28448.
5. Coulter, E. D., and Kurtz, D. M. Jr. (2001) *Arch. Biochem. Biophys. 394*, 76−86.
6. Voordouw, J. K., and Voordouw, G. (1998) *Appl. Environ. Microbiol. 64*, 2882−2887.
7. Dos Santos, W. G., Pacheco, I., Liu, M.-Y., Teixeira, M., Xavier, A. V., and LeGall, J. (2000) *J. Bacteriol. 182*, 796−804.
8. Poole, L. B., Reynolds, C. M., Wood, Z. A., Karplus, P. A., Ellis, H. R., and Calzi, M. L. (2000) *Eur. J. Biochem. 267*, 6126−6133.

9. Coulter, E. D., Shenvi, N. V., and Kurtz, D. M. (1999) *Biochem. Biophys. Res. Commun. 255*, 317−323.
10. Lumppio, H. L., Shenvi, N. V., Summers, A. O., Voordouw, G., and Kurtz, D. M. (2001) *J. Bacteriol. 183*, 101−108.
11. Pianzzola, M. J., Soubes, M., and Touati, D. (1996) *J. Bacteriol. 178*, 6736−6742.
12. Silva, G., LeGall, J., Xavier, A. V., Teixeira, M., and Rodrigues-Pousada, C. (2001) *J. Bacteriol. 183*, 4413−4420.
13. Hatchikian, E. C., and Henry, Y. A. (1977) *Biochimie 59*, 153−161.
14. Hardy, J. A., and Hamilton, W. A. (1981) *Curr. Microbiol. 6*, 259−262.
15. Tavares, P., Ravi, N., Moura, J. J. G., LeGall, J., Huang, Y. H., Crouse, B. R., Johnson, M. K., Huynh, B. H., and Moura, I. (1994) *J. Biol. Chem. 269*, 10504−10510.
16. Verhagen, M. F. J. M., Voorhorst, W. G. B., Kolkman, J. A., Wolbert, R. B. G., and Hagen, W. R. (1993) *FEBS Lett. 336*, 13−18.
17. Coelho, A. V., Matias, P., Fülöp, V., Thompson, A., Gonzalez, A., and Coronado, M. A. J. (1997) *Biol. Inorg. Chem. 2*, 680−689.
18. Yeh, A. P., Hu, Y., Jenney, F. E., Adams, M. W. W., and Rees, D. C. (2000) *Biochemistry 39*, 2499−2508.
19. Clay, M. D., Jenney, F. E., Jr., Hagedoorn, P. L., George, G. N., Adams, M. W. W., and Johnson, M. K. (2002) *J. Am. Chem. Soc. 124*, 788−805.
20. Coulter, E. D., Emerson, J. P., Kurtz, D. M., Jr., and Cabelli, D. E. (2000) *J. Am. Chem. Soc. 122*, 11555−11556.
21. Lombard, M., Houée-Levin, C., Touati, D., Fontecave, M., and Nivière, V. (2001) *Biochemistry 40*, 5032−5040.
22. Nivière, V., Lombard, M., Fontecave, M., and Houée-Levin, C. (2001) *FEBS Lett. 497*, 171−173.
23. Abreu, I. A., Saraiva, L. M., Soares, C. M., Teixeira, M., and Cabelli, D. E. (2001) *J. Biol. Chem. 276*, 38995−39001.
24. Mathé, C., Mattioli, T. A., Horner, O., Lombard, M., Latour, J. M., Fontecave, M., and Nivière, V. (2002) *J. Am. Chem. Soc.* 124, 4966−4967.
25. Mäntele, W. (1993) *Trends Biochem. Sci. 18*, 197−202.
26. Siebert, F. (1993) *Methods Enzymol. 246*, 501−526.
27. Deacon G. B., and Phillips, R. J. (1980) *Coord. Chem. Rev. 33*, 227−250.
28. Nara, M., Torii, H., and Tasumi, M. (1996) *J. Phys. Chem. 100*, 19812−19817.
29. Moss, D. Nabedryk, E., Breton, J., and Mäntele, W. (1990) *Eur. J. Biochem. 187*, 565−572.
30. Susi, H. (1969) in *Structure and Stability of Biological Macromolecules* (Tunasheff, S. N., and Fasman, G. D., Eds.) Vol. 2, pp 575−663, Marcel Dekker, New York.
31. Berthomieu, C., Boussac, A., Mäntele, W., Breton, J., and Nabedryk, E. (1992) *Biochemistry 31*, 11460−11471.
32. Hienerwadel, R., and Berthomieu, C. (1995) *Biochemistry 34*, 16288−16297.
33. Noguchi, T., Inoue, Y., and Tang, X.-S. (1999) *Biochemistry 38*, 399−403.
34. Venyaminov, S. Yu, and Kalnin, N. N. (1990) *Biopolymers 30*, 1243−1257.
35. Barth, A. (2000) *Prog. Biophys. Mol. Biol. 74*, 141−173.
36. Maeda, A., Sasaki, J., Shichida, Y., Yoshizawa, T., Chang, M., Ni, B., Needleman, R., and Lanyi, J. K. (1992) *Biochemistry 31*, 4684−4690.
37. Chirgadze, Y. N., Fedorov, O. V., and Trushina, N. P. (1975) *Biopolymers 14*, 679−694.
38. Venyaminov, S. Y., and Kalnin, N. N. (1990) *Bioploymers 30*, 1259−1271.
39. Dioumaev and Braiman, M. S. (1995) *J. Am. Chem. Soc. 117*, 10572−10574.

BI020344X